Projects in the Design and Construction of a Scanning Tunneling Microscope and UHV Sample Analysis Chamber

Author: Patrick W Oakes

Undergraduate Honors Program

Physics

Projects in the Design and Construction of a Scanning Tunneling Microscope and UHV Sample Analysis Chamber

By

Patrick W. Oakes

Submitted in partial fulfillment of the requirements
the degree of

B.S.

Projects in the Design and Construction of a Scanning Tunneling Microscope and UHV Sample Analysis Chamber

Abstract

Three projects have been undertaken during the design and the construction of a scanning tunneling microscope. The first project focuses on a method of testing the movement of piezoelectric ceramics by means of a modified Michelson interferometer. These tests determine the magnitude and the direction of motion on the scale of a few angstroms. These piezos are then used in moving the tip of the STM. The second project concerned the design of a surface analysis chamber to be used for thin film depositions. This chamber will operate at UHV levels and will produce samples to be examined by the STM. The final project dealt with the construction and testing of a feedback loop to be used in the e-beam heater during thin film depositions. This box monitors the current between the sample and the source modifying the voltage across the filament to ensure the current between the two remains constant, ensuring a constant deposition rate.

Projects in the Design and Construction of a Scanning Tunneling Microscope and UHV Sample Analysis Chamber

Patrick W. Oakes
Advidor: Prof. Vidya Madhavan
4/30/04

Chapter I

Introduction

The first Scanning Tunneling Microscope (STM) was built in 1982 by Gerd Binnig and Heinrich Rohrer while working for IBM[1]. The process involves bringing the tip of the microscope close enough to the surface of a sample to allow electrons located in the tip and the sample to tunnel between them. By measuring the current that results from this tunneling, images of the surface can be obtained. These images can have resolutions on a scale of a few angstroms, a feat previously unobtainable. This technique opened a variety of new research opportunities in the area of surface science. Today the STM is a vital part of any laboratory seeking to further explore and understand the surface of materials.

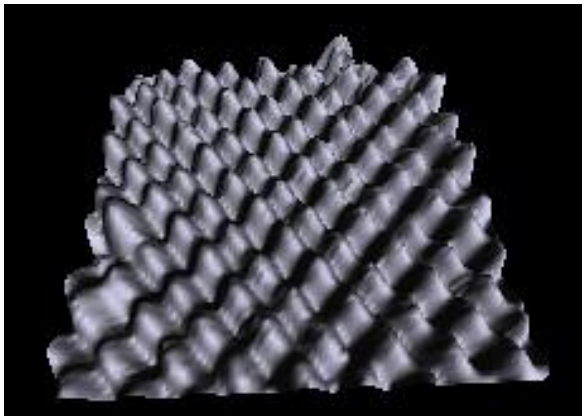

Figure 1.1 - Atomic resolution (30Å X 30 Å)
STM image of a Si(100) surface[2]

This thesis is the culmination of my work with one such group which is in the process of building their STM. This first chapter serves as an introduction to the group and provides the backdrop and the motivation for my own work. The second, third and fourth chapters highlight the three specific areas in which I focused my attention.

Following these chapters there are a number of appendices that provide the theory for the work presented here.

1.1 The Madhavan Group's STM

The Madhavan group is currently in the process of designing and building its own STM. The entire system will be maintained in an ultra high vacuum (UHV). The microscope will operate at pressures of 2×10^{-10} torr and below. This vacuum is achieved through a tiered system of pumps and heating of the chamber that removes as much of the gas as possible from the system. The benefits of working in extremely low pressures are that samples will remain cleaner for longer periods of time allowing for greater and more extensive analysis.

The STM is being placed in a new lab that is being constructed in the basement of the building. The lab is placed in the basement of the building in order isolate the STM from a variety of interference and vibrations. Vibrations in the building can be caused by any number of phenomena, including wind and pedestrian traffic. The STM is incredibly sensitive to these small vibrations on account of the small scale on which it operates.

The microscope itself will be placed into a dewar filled with liquid helium. This will reduce the operating temperature of the STM down to 4 Kelvin Operation at low temperatures provides a number of advantages. Thermal activity at 4 Kelvin is very small allowing for both the manipulation and study of single atoms on a surface. At room temperature a single atom on the surface would never sit still for a period long enough to make measurements. Spectroscopic resolution is also greater at lower temperatures. This is due to the fact that the Fermi surface is temperature dependent and as the temperature is raised the amount the Fermi surface is smeared also increases. In addition to these two effects, low temperatures reduce thermal noise and also provide stability in the ambient temperature of the chamber.

In order for tunneling to occur the tip must be positioned close to the surface of the sample. Positioning and movement of the tip is controlled through the use of piezoelectric crystals. These crystals can be deformed in a controllable manner through the application of certain electric fields. Two different piezoelectric crystals are employed in the STM. One set of piezos will provide the movement for the walker to

position the STM tip above the sample. Once the tip is in position the second piezoelectric crystal is employed. This crystal will be in the shape of a tube and is capable of movement in all three orthogonal directions. The movement in the x and y planes will serve to scan the tip across the surface while the motion in the z plane will be used to maintain a constant current between the tip and the sample. The theory of piezoelectricity is discussed further in Appendix B.

Operating the STM requires a number of different electronic devices. The software and electronics control the coarse approach of the tip, the scanning motion of the tip and also the measurement of the tunneling current. Some of the devices are being purchased commercially but a few are being built from scratch.

Attached to the STM chamber will be a sample analysis chamber. It will operate at room temperature but will still be maintained in UHV. Semiconducting, metallic thin film samples will be prepared in this chamber. This chamber will also contain the equipment needed to do a variety of analysis including low energy electron diffraction (LEED) and Auger electron spectroscopy. Once the samples are prepared they will be transferred directly to the STM by means of a system of manipulators inside of the chamber. This will allow us to complete the sample transfer without breaking the vacuum of the system.

1.2 Projects

During the past year I have been working on three projects within the Madhavan group. These have been highlighted in the schematic of the system below.

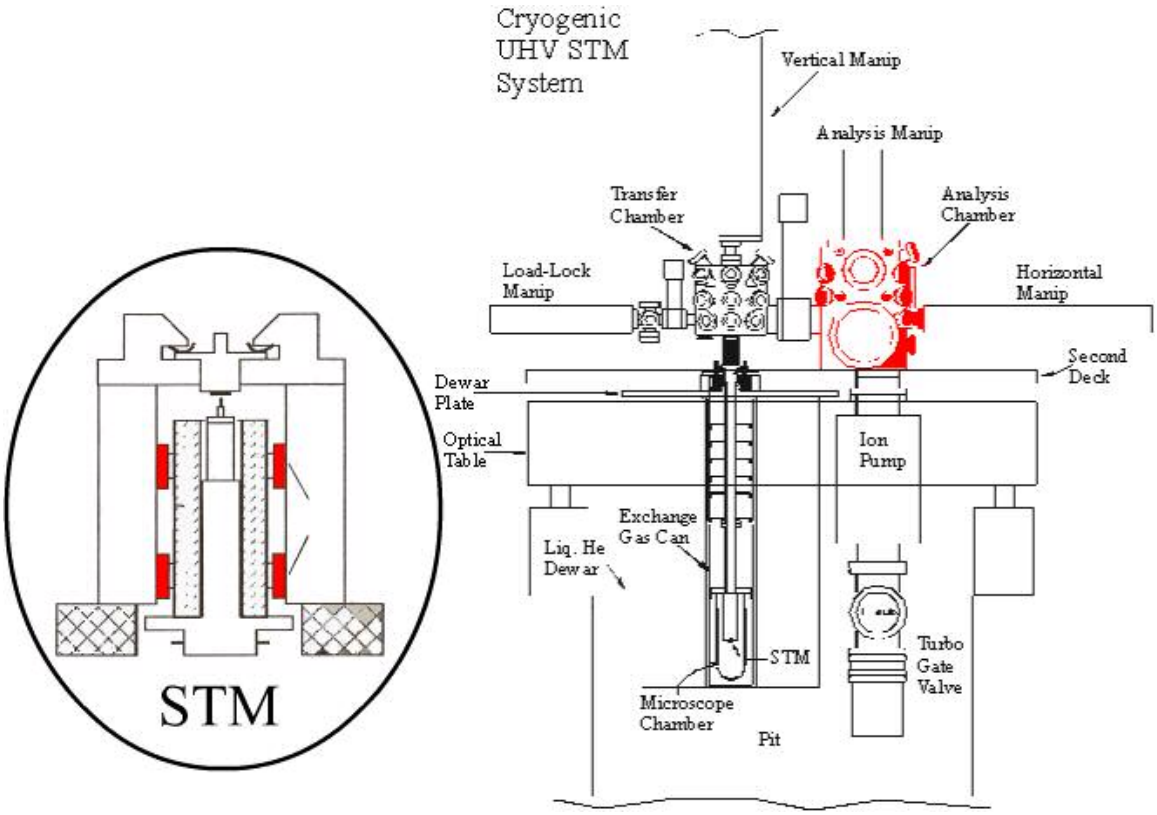

Figure 1.1[3] The STM with all of its components. The particular projects focused on in this thesis are highlighted in red. The first project tested the piezo stacks actually located in the STM. The second project was the design of the analysis chamber. The third project, not shown, was building a feedback box for the electronics.

I will briefly describe each project here before using the following chapters to discuss in detail the work and experiments involved with each section.

The first project focused on the piezoelectric ceramics that are used to move the tip to within tunneling range of the sample surface. These piezoelectric crystals shear when placed in the presence of an electric field. My objective was to design a system to test the movement of these crystals and to determine which ones should be used in the STM. Testing was done using an interferometer with one of the mirrors located on top of the piezo. As the piezo moved the interference pattern created by the interferometer changes. By analyzing this movement an accurate assessment of the motion of the piezo could be made. Once the useful piezos were identified, they were set aside to be glued together in the stacks that are to be used in the STM.

The second project was to build the UHV surface analysis chamber that will be used for thin film depositions. This chamber will ultimately be attached directly to the STM but should also function as a stand alone chamber. An e-beam heater inside of the chamber will evaporate the source to be deposited. A series of manipulators and screens will be used to control the evaporation while a crystal monitor will measure the actual deposition rate of the source.

The third and final project focused on the control electronics for the e-beam heater. In the process of depositing thin films by means of an e-beam heater a constant current must be maintained between the filament and the source to be evaporated. To accomplish thistask a feedback loop must be installed in the circuit. This feedback loop analyzes the current and changes the voltage across the filament accordingly to maintain the constant current in the larger circuit. My job was to actually build and test the circuit for use in the e-beam heater.

Chapter II

Measurement of Piezoelectric Motion

The piezoelectric effect is the process of inducing a mechanical stress in a crystal by means of applying an electric field (See Appendix B). Our purpose for discussing it here lies in the pivotal role it plays in the functioning of the STM. Because the motion of the piezos is so small, it is possible to use them to manipulate the tip of the STM over very small areas of the sample surface. Since the current is related exponentially to the distance between the tip and the sample (see Appendix A), an image can be created by measuring the fluctuations of the current as the tip moves over the surface. There are two different piezoelectric crystals that are used in the STM. The type that is the focus of this experiment is a set of six stacks of square piezoelectric ceramics attached between the body of the STM and the tip holder which control the coarse positioning of the tip. These stacks consist of four small square piezos bonded together in a specific pattern. When combined properly all the piezos shear in the same direction producing a movement with a magnitude four times greater than a single crystal. All the piezos in this experiment exhibit a single shear motion when a voltage is applied through the two large faces of the piezo.

An experiment was developed to test the piezoelectric crystals that had been purchased before they were used in the STM. This is important because often the piezos purchases do not behave as specified by the manufacturer. The test measured the direction and the magnitude of the shear. In order to be of use the piezos have to show a shearing motion in a single direction and have a magnitude of movement of roughly 330 x 10^{-12} m/V. The material used in this experiment was a lead zirconium titanate referred to as EBL #4. The pieces were all machined to be 0.300” x 0.300” x 0.02” in dimension. Nickel polished electrodes were applied to both of the large faces of the piezos and the direction of the shear was marked by a small black arrow on the surface of the positive electrode. The depoling voltage of this piezoelectric material is 20 volts per 1/1000 of an inch. For this particular geometry that translates to a depoling voltage of 400 V in the

direction of the polarization. In the direction opposite to the polarization the depoling voltage is exactly half the direction of polarization and is thus 200 V. For our purpose the voltage was only applied in the direction of the polarization and a limit of 350 V was never surpassed as to ensure that the piezos were never depoled.

The piezos were tested by placing the crystals in a modified interferometer and studying the movement of the interference pattern created. Because the interference pattern is a product of optical interference, movements of the mirror with magnitudes on the order of nanometers produce visible alterations to the pattern. By observing the change in this pattern the magnitude and the direction of the motion of the piezo was calculated.

2.1 Experimental Technique

The setup of this experiment was based upon the Michelson Interferometer (Figure 2.1). A beam of light is passed from the source through a convex lens. From the lens the light travels to a half silvered mirror located in the middle of the interferometer. This half silvered mirror functions as a beam splitter, reflecting half of the light incident upon it at a right angle, while allowing the other half to pass through the mirror unimpeded. At this point there are now two beams of light. Beam 1, which is reflected by the beam splitter, is reflected off a stationary adjustable mirror, that sends the beam directly back to the beam splitter. Beam 2, which passes through the beam splitter without being reflected, bounces of a moveable mirror, and is sent back to the beam splitter. The two beams arriving back at the beam splitter are then recombined into a single beam. Since the beams originated from the same source they are coherent and produce an interference pattern which is visible upon the screen.

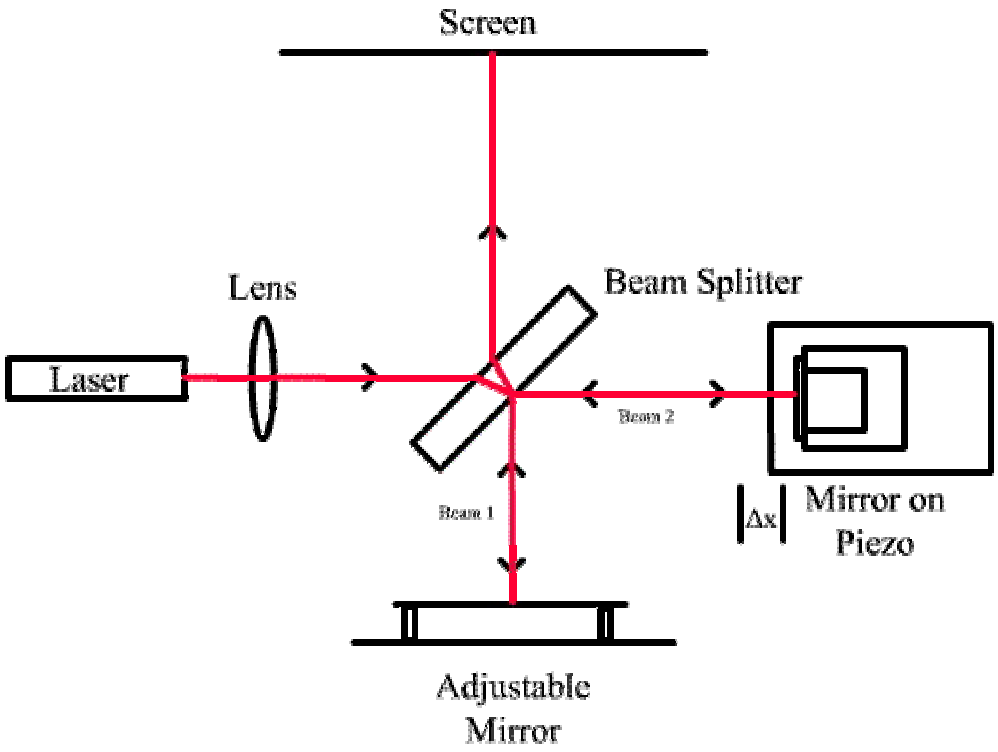

Figure 2.1 – The Michelson Interferometer setup for testing the piezoelectric crystals.

The interference pattern, when centered correctly, produces a series of concentric rings. These are a series of minima and maxima. The red rings represent the maxima and the black rings represent the minima.

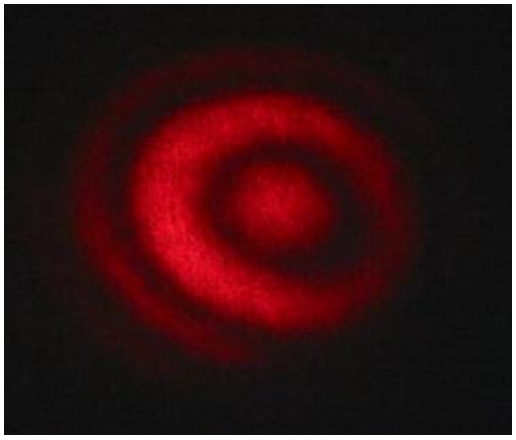

Figure 2.2 – The actual interference pattern.

A fringe in this thesis is being referred to as each separate colored ring. Based upon the wave theory of light the distance between the center of each maxima is equivalent to one wavelength of the incident source. By counting the number of rings that pass through the center of the interference pattern during a movement, the magnitude of the movement can be calculated. A movement of one wavelength on the screen corresponds to a physical difference of a half wavelength in the path length. This factor of two is the result of the fact that the light travels the path difference, Δx (Figure 2.1), once on its way to the mirror and once again on its way from the mirror. An accurate measurement can thus be made simply by counting fringes. The more fringes that are counted, the more accurate the process becomes.

The adjustable mirror consists of a mirror attached by a spring and two screws to a base plate. The two screws are at opposite corners and by tightening or loosening the screws it is possible to make minor adjustments to the direction the mirror is facing thus allowing one to effectively aim the beam that is being reflected. This is vital to our ability to realign the two split beams creating the interference pattern. The two beams must lie along exactly the same path in order to interfere and create the interference pattern.

The movable mirror for the Michelson interferometer is usually a simple mirror attached to a base plate. The base plate is then attached by some mechanism that allows the mirror to move linearly along the axis of the beam of light, thus altering the path length. In our setup the mirror was placed on top of the piezoelectric crystal (figure 2.3). When a field is applied to the crystal it shears, moving the mirror and changing the path length. A simple holder for the mirror was machined. The base consisted of a plastic block of macor with a hole drilled in the bottom so as to firmly attach it to the interferometer. Upon the macor block we placed a small block of aluminum. This aluminum block was secured by means of a screw in a recessed hole in the bottom of the macor. A separate freestanding rectangular block of copper was also machined with a width and depth to match the piezo squares. In both the aluminum and copper blocks a tapped hole was drilled. The tapped holes serve as the points for attaching the leads to the voltage source.

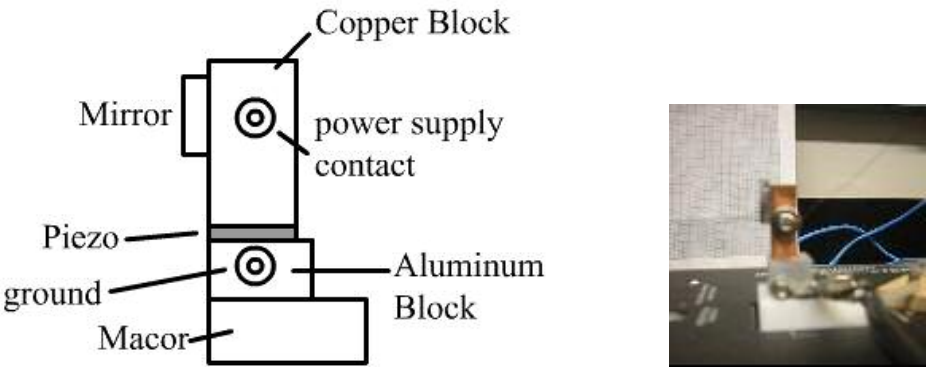

Figure 2.3 – The picture mirror setup used for the piezo. As the piezo shears the mirror moves backwards or forwards. The actual mirror is shown on the right.

The macor block provides a means of attaching the mirror to the interferometer while insulating it from the voltage that is going to be applied to the two metal blocks on top. This was important because the interferometer used was solid metal and would very easily conduct the high voltages that we used in the experiment, thus creating the potential for danger. The voltage source was attached to the two metal blocks by means of a BNC cable with one of the end connectors cut off. The plastic coating was removed and the metal sheathing of the wire pulled back. The sheathing was attached to the screw on the block of aluminum providing a ground for our circuit. The central wire in the BNC cable was attached to another screw set in a piece of wood attached to the interferometer. From this screw an incredibly fine wire, 29 AWG, was run to the screw in the copper block. The central BNC wire was not attached directly to the copper block for fear of the wire being to stiff and inhibiting the movement of the block on top of the piezo. By using a smaller gauge wire the stiffness of the wire is greatly reduced removing the problem. A small mirror, 0.5” in diameter, was attached to one face of the copper block by means of superglue. The piezoelectric piece was placed on top of the aluminum block and the copper block was then balanced on top of the piezoelectric piece.

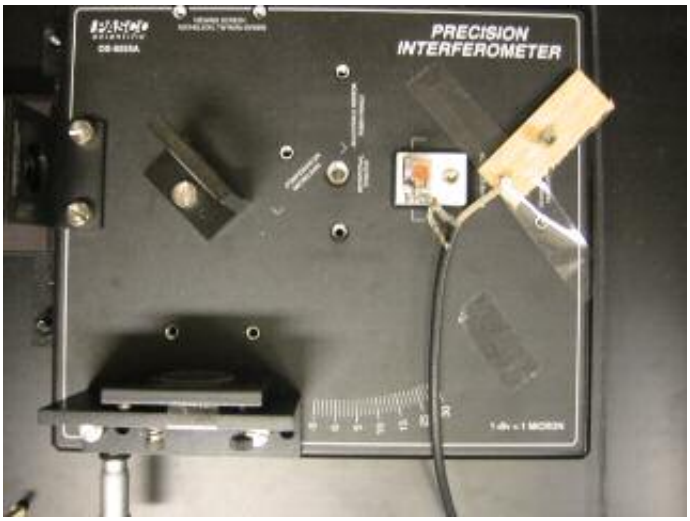

Figure 2.4 – The actual interferometer used. The laser is just out of the picture on the left. The beam splitter is in the center. The adjustable mirror is at the bottom of the picture and the piezo mirror is just to the left of the piece of wood. The screen is just out of the picture at the top of the interferometer.

The light source that was used in the experiment was a 633 nm standard HeNe laser source. It runs on a input of 12 VDC and 0.7 A. The power supply consisted of a Pacific Precision Instruments high voltage power supply that outputs up to 2 kV. For our purposes the supply was arranged to output a negative voltage between 0 and -350 volts so as to not depole the piezos. A screen was put in place approximately 2 ft from the beam splitter.

The method followed for testing the piezos consisted of three different measurements. The piezos were sent from the manufacturer marked by an arrow indicating the direction of shear on the positive electrode. Since a negative voltage was being applied the arrow was always placed face down so that the arrow face was pressing against the aluminum block. The first measurement was made with the arrow pointing towards the beam splitter. The second measurement was made with the arrow rotated 180° from the first measurement. The final measurement was made with the arrow rotated back 90° so that it pointed towards the screen. The movement in the interference

pattern and the applied voltage was recorded for each measurement. Each piezo was tested at least twice.

Each time the copper block was placed on top of the piezo a centering procedure was followed. A flat metal spacer was held pressed against the front of the block of the aluminum. A plastic paddle was then used to push the piezo, with the copper block on top of it, flush against the metal spacer. This ensured that the face of the copper block with the mirror on it was flush with the piezo and the block of aluminum and also that the whole system was normal to the incoming beam.

Measurements of the system were made based upon the observations of the movement of the interference pattern. A piece of finely spaced graph paper was placed over the wall where the interference pattern was created giving a reference frame by which to judge the movement. Once the interference pattern was visible on the screen the adjustable mirror was positioned so that the pattern was centered and a circular pattern of rings was visible. A voltage of -350 V was applied and the movement was recorded on the data sheet (Appendix C). A one fringe movement correlated to a movement of a red center dot to a black center dot of roughly the same size. The best judgment of the observer was used to approximate the movement to within a quarter fringe. The direction of the movement of the fringes was also recorded. An inward motion indicated that the fringes collapsed on each other in the center of the pattern. An outward motion meant the fringes grew out from the center of the pattern.

2.2 Experimental Results

The following piezos were deemed to be good and bad:

Good Piezos			
2	20	36	N11
4	23	38	N13
8	26	39	N15
10	27	40	N17
13	29	46	N19
15	31	50	N23
17	32	N8	N24
Total: 29			

Bad Piezos	
11	49
12	N1
33	N10
34	N21
37	N22
47	
Total: 11	

Figure 2.5 – The list of the piezos that were determined to be good and bad. The numbers refer to the number written on the bag containing each piezo.

The direction of the fringe movements indicates the direction of the shear. As predicted by the theory (Appendix B, Figure B.2) an inward fringe movement in the first orientation tested indicated a shortening of the difference in the path length. This was confirmed by means of pushing gently on the macor block in the direction of the beam splitter. This gentle pushing produced the same inward fringe movement. An inward movement therefore indicates a shear in the direction of the beam splitter and an outward movement indicates a shear in the direction away from the beam splitter.

For our experiment certain requirements were placed on the movement of the piezos. The piezo had to shear inward on the first orientation, outward on the second orientation and had to show little to no movement in the third orientation. Ideally the piezos should have moved roughly ¾ of a fringe at a voltage of -350 V.

$$\tfrac{3}{4}\text{fringe} = \tfrac{633}{2} * \tfrac{3}{4} = 237.38\text{nm} \tag{2.1}$$

From this we can calculate the change in the path length.

$$\Delta x = \tfrac{237.38}{2} = 118.7\text{nm} \tag{2.2}$$

This in turn translates to a motion of

$$\frac{118.7\text{ nm}}{350\text{ V}} = 339x10^{-12}\ \text{m}/\text{V} \tag{2.3}$$

This corresponds nicely with the given value for the movement of the piezo of 330 x 10^{-12} m/V. Movement between ½ a fringe and 1 fringe were tolerated.

Of this group 29 out of 40, or 72.5%, behaved acceptably. This number, however, is much higher than the actual success rate. Through the process of perfecting the testing procedure, 24 piezos from the original batch of 50 were deemed to be unacceptable and were returned to the company to be replaced. The 26 piezos labeled only with a number are the remaining piezos from this batch. All piezos with the label N followed by a number were from the new set of piezos. These new piezos were also screened by another tester.[4] Only those piezos which were though to possibly be well behaved were passed on to be tested by me. Of these 24 new piezos, only 12 were considered to possibly be acceptable and were tested by me.

Thus out of the first batch of piezos, 20 of 50, or 40% behaved in the expected manner. Of the second batch of piezos, 8 of the 24, or 33.3% behaved acceptably. Overall we have had a success rate of 29 out of 74 piezos, or 39.2%. This low success rate has justified the need for testing the material.

In conclusion, the method of the piezo testing was successful. The interferometer allowed us to measure movements of roughly 115 nm with a good accuracy. The test was consistent and produced repeatable results. Despite the poor percentage of acceptably behaving piezos, the test overall was successful in identifying those piezos which should be used in the STM.

Chapter III

Design of an Ultra High Vacuum Chamber for Thin Film Depositions

An STM is only as useful as the samples which it studies. Sample preparation is a vital component of any STM. The study of different surface effects requires a number of different preparation techniques and arrangements. One such technique depends upon depositing thin films onto a given substrate by evaporating a source material. Deposition is a delicate process that must be accurately controlled in order to create pure and nicely ordered samples.

These films are used in a variety of different ways. The simplest method is to deposit epitaxial layers upon the entire surface of the substrate. These layers are well ordered periodic structures upon which surface effects can be analyzed. The periodic structure of these layers is also useful for growing other crystals using the layer as a base. Different substrates can produce different periodic structures in the deposited film. Depending on the choice of the substrate the structure of the layer can be controlled. Other interesting effects can be observed by using masks on the substrate to grow islands of materials. These can be used to explore local surface effects. Impurities can also be introduced into the system to create further effects on the surface and in the periodicity. These are just a few of the uses of thin films in the area of surface science. The goal of this project was to be able to build a chamber with all the necessary equipment to deposit thin films on a substrate.

3.1 The Vacuum Chamber

The chamber is designed with the intent of accommodating not only the equipment used in the thin film deposition but also any other analysis equipment that might be purchased in the future. A chamber designed by Nor-Cal was determined to suit all of the needs of this project. This particular chamber is made of 304 SS and was designed specifically with the idea of sample analysis in mind. It can be reduced to UHV

levels and has 18 ports to accommodate all of our equipment. The chamber and its dimensions are given in figure 3.1. All dimensions are listed in inches.

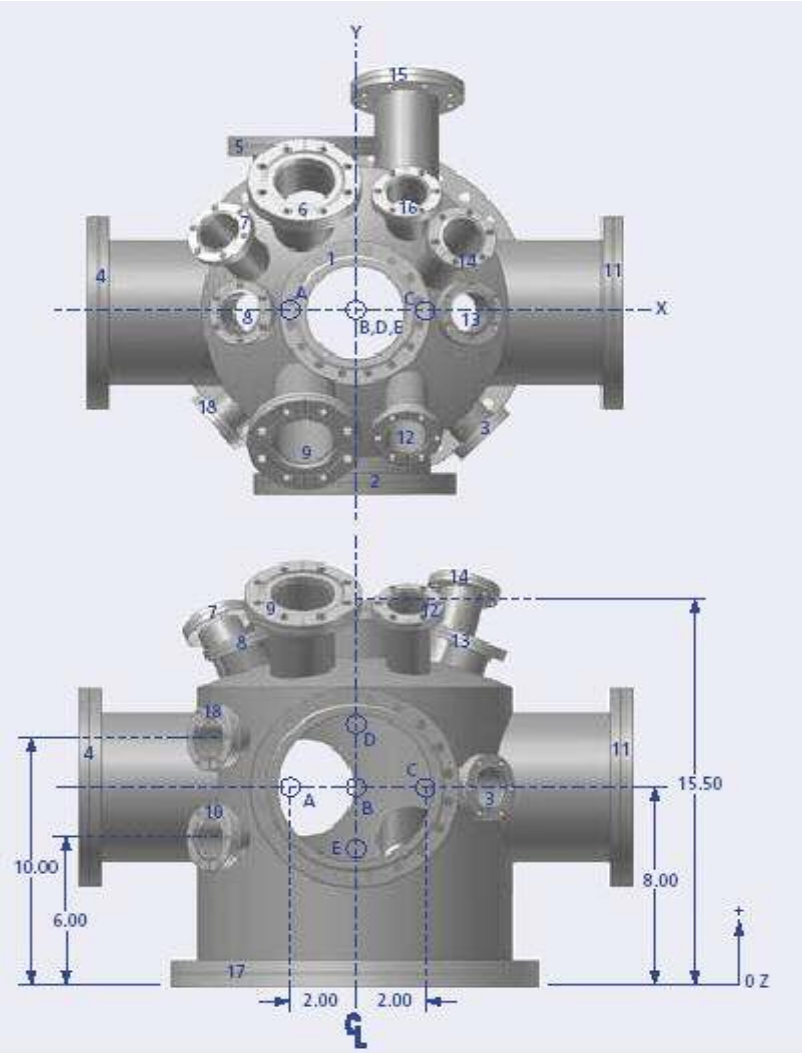

Figure 3.1 – The vacuum chamber designed by Nor-Cal.[5]

This chamber has three major focal points and two secondary focal points. The main focal points are labeled A, B and C, and all lie along the main horizontal axis through the center. B is located in the exact center of the chamber while A and C are offset by 2 inches to either side. There are six different ports focused on point A and another six ports focused on point C. This is incredibly useful because it allows for two different setups to be utilized at the same time. One process can be conducted at point A,

the sample can be rotated and another process performed at point C. The secondary foci are located at points D and E. Each of these points is the focus of only one small port on the side of the chamber.

Port Number	*Flange Size*	*Focal Point*	*Focal Length*	*Polar Angle*	*Azimuthal Angle*
1	6.00	B	7.50	0°	NA
2	8.00	B	7.50	90°	90°
3	2.75	B	7.25	90°	45°
4	8.00	A	8.50	90°	180°
5	6.00	A	7.25	90°	270°
6	4.50	A	8.50	40°	270°
7	2.75	A	8.25	35°	225°
8	2.75	A	6.50	23°	180°
9	4.50	A	9.50	35°	90°
10	2.75	E	7.25	90°	140°
11	8.00	C	8.50	90°	0°
12	2.75	C	9.00	35°	90°
13	2.75	C	6.50	23°	0°
14	2.75	C	9.00	25°	305°
15	4.50	C	10.00	110°	270°
16	2.75	C	7.75	40°	270°
17	14.00	B	8.00	180°	NA
18	2.75	D	7.25	90°	140°

Figure 3.2 – Port characteristics for the chamber. All dimensions are in inches.

The focal points encompass a variety of different sizes and angles (see above). Nine of the ports are located on the top of the chamber. There are three 8” flanges on the sides along with two slightly smaller ones slightly offset from the center. The chamber is dominated by a large 14” flange taking over the entire bottom of the chamber cylinder. This is ideal because it allows us to use a reducer and attach any size pump that we choose maximizing the conductance. This will improve our pumpdown times and make it easier and quicker to reduce the pressure of the chamber down to UHV.

The seal along these ports is of the utmost importance. There are many different types of seals that are available for connecting vacuum equipment. They all have their advantages and their disadvantages. This particular system was designed around the ConFlat (CF) flange. An OFHC copper gasket is placed between the knife-edges of each flange. As the screws on the face of the flange are tightened the knife-edge bites into the

softer copper gasket creating an air tight seal. The advantage of this is that small defects along the knife-edge or the gasket are compensated by the knife-edge biting into the copper. This is very helpful in preventing leaks. The drawback of this flange type is that it is next to impossible to use the copper gaskets more than one time because they have been imprinted upon by the unique knife-edge of that flange.

Different procedures are followed when tightening the bolts on the flanges depending on the size of the flange (Figure 3.3). On the small 2 ¾" flange the bolts can be tightened in a sequential sequence. With the 4" and 6" flange a slightly different process is employed. Bolts are inserted and tightened by using a balancing method. For every bolt inserted the next bolt is the one directly across the face of the flange. The next two bolts then progress further around the circle until the entire face has been secured. With the 8" and larger flange sizes the process becomes even more complicated, basing itself upon a triangle. A triangle of bolts is secured before shifting one bolt hole forward at each point for successive bolts. This is best illustrated in the diagram below.

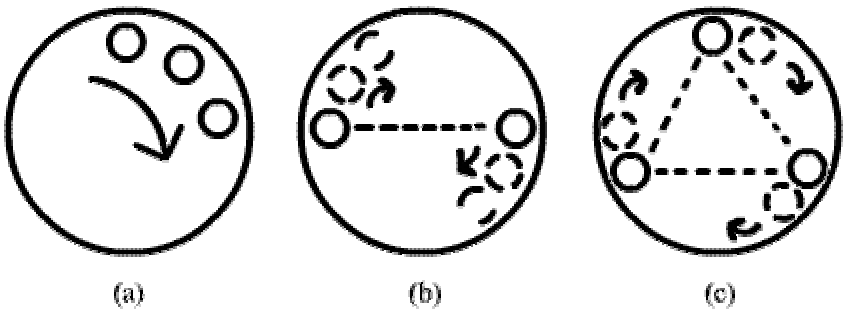

Figure 3.3 – The different patterns followed when bolting on the flanges. (a) For 2 ¾" flanges. The bolts are tightened sequentially around the circle. (b) For 4.5" and 6" flanges. The bolts are tightened in opposing sequences as they progress around the circumference. (c) For 8" flanges and larger. This method uses a triangle pattern for progressing around the edge. After each triangle is completed the pattern is shifted one bolt and begun again.

These processes are followed so as to ensure that the flanges are tightened evenly across the copper gasket. For all the flanges, the bolts are first hand tightened in order according to the proscribed method. Once this is done the bolts are tightened slightly

using a wrench, moving around to all the bolts before returning to the first bolt to tighten it further. This process is repeated until the bolts have all been sufficiently tightened. If this method was not followed we would stand the chance of ruining the copper gasket and creating an imperfect seal which would allow for leaks to occur and thereby make UHV impossible to achieve.

3.2 The Crystal Monitor

The crystal monitor allows us to monitor the rate of deposition inside of the chamber. It utilizes the inherent resonant frequencies of quartz. The frequency at which this oscillation occurs is a direct result of the thickness of the quartz. A feedthrough is attached to a port on the chamber positioning the sensor near the sample to be coated by a thin film. Both the sample and the sensor head are deposited on. As the sensor is coated the thickness of the quartz is altered, changing the frequency at which it oscillates. This change in frequency is continually measured and used to calculate the change in the thickness of the quartz and thus also the thickness of the film deposited.

The crystal sensor and the e-beam heater are the only pieces of equipment that are actually located in the vacuum (Figure 3.4).

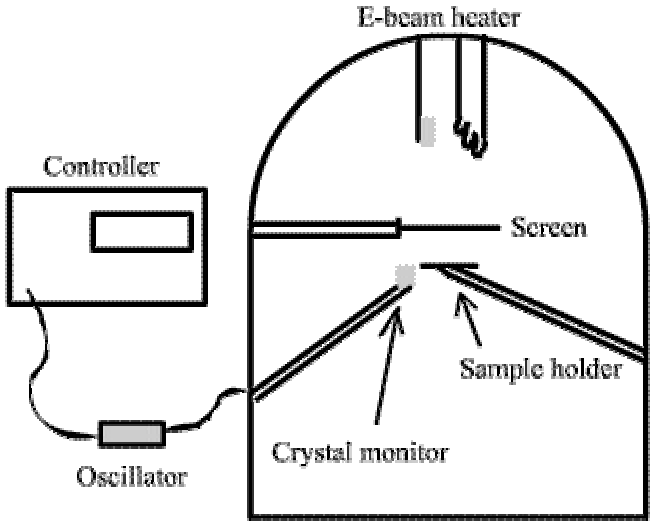

Fig 3.4 of the monitor in vacuum

A connector called a microdot is located on the base of the feedthrough flange of the sensor. This connector allows for the sensor to pass information back to an oscillator which interprets the frequency and sends it out to the controller. The controller then calculates the thickness of the film and sends it to the display on the front of the box. It is from this method that we are able to have accurate control over the thickness of films deposited.

3.3 Rough and Turbo Pumps

Two different pumps will be used to lower the pressure inside of the chamber down to UHV levels. The rough pump is responsible for lowering the pressure from atmosphere down to about 10^{-3} torr. At this point the turbo pump takes over and lowers the pressure down to 10^{-10} torr. In order to reach the lowest pressures possible the chamber must be heated in order to remove the gasses trapped inside of the metal. Through the full process of pumping and heating the UHV level is achieved.

The rough pump in our system is a two stage rotary vane pump. This pump operates on the principle of using positive displacement to move the gas molecules out of the chamber and into the atmosphere. The vanes sweep out the particles that come into the small chamber inside of the pump. Because the pressure levels attained by this method are not too low, the gasses can be evacuated directly to the atmosphere.

When the turbo pump takes over the flow of gas molecules in the chamber behaves as a molecular flow. Molecules are removed by imparting kinetic energy in a particular direction. This is accomplished through means of many closely spaced rotating discs that have angled slots cut in them. As the molecules hit the angled faces of the slots they are pushed further out of the chamber. The turbo pump is connected directly to the rough pump which then exhausts the gas out to the atmosphere.

3.4 Layout of Components for Thin Film Deposition

Our setup for the thin film deposition was planned according to the following schematic. Three large viewports are attached to port numbers 4, 2 and 11 (Figure 3.1). These allow us to view what is going on inside the chamber. The turbo pump is attached to port number 17 by means of a nipple that reduces the 14” flange to a 6” flange. The

nipple will pass through a hole in the table allowing the turbo pump to hang from the bottom of the chamber. The rough pump will be attached directly to the turbo pump under the table.

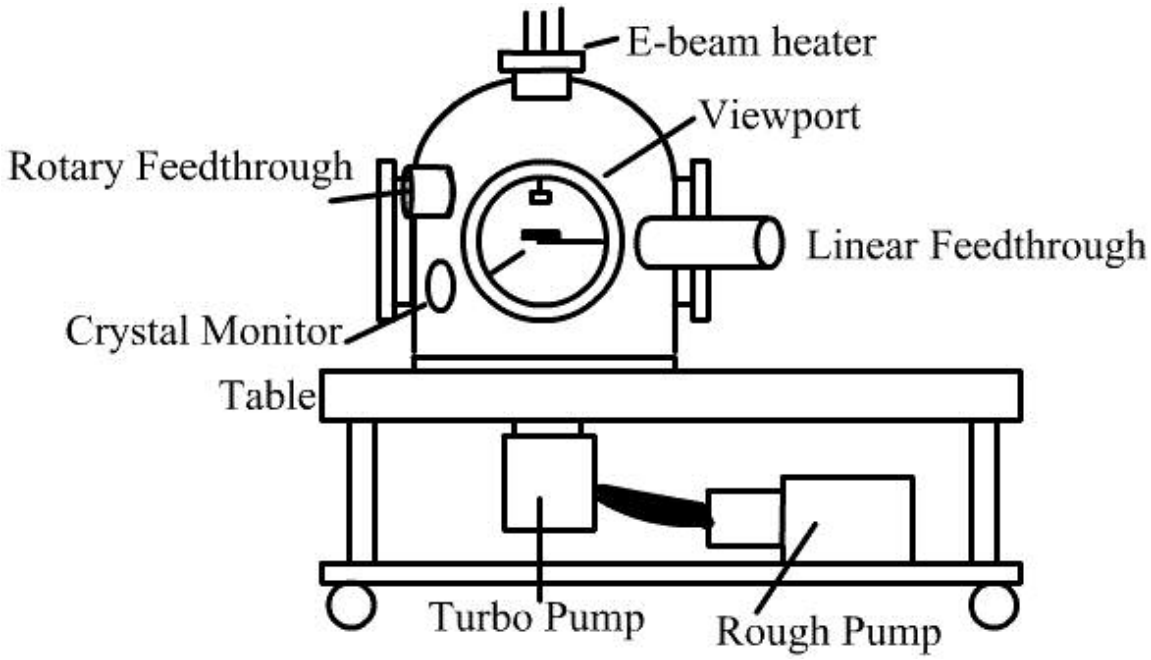

Figure 3.5 – The setup of the analysis chamber. The pumps are under the table. The e-beam heater comes down through the top center port. All the other instruments come in through the side ports. Everything is monitored through the viewports.

The e-beam heater is inserted through the top of the chamber in port number 1. Because the e-beam heater is attached by means of a 2 ¾" flange a zero-length reducer is going to be used on port number 1. The sample is to be held on the linear feedthrough attached through port number 3. The crystal monitor is inserted through flange 10 and is positioned underneath the sample. The rotary feedthrough is fixed with a screen and attached to port number 18. This will block the source allowing us to control the length of time the substrate will be exposed to the evaporated source. The rest of the ports are covered with blank flanges that will provide us with the vacuum seal.

Chapter IV

Control Electronics for E-Beam Deposition

The e-beam heater is a crucial component in the process of performing thin film depositions. It operates under the principle of placing a filament close to the source, causing it to evaporate. A large voltage (2 kV) is passed through the circuit, a diagram of which can be seen below.

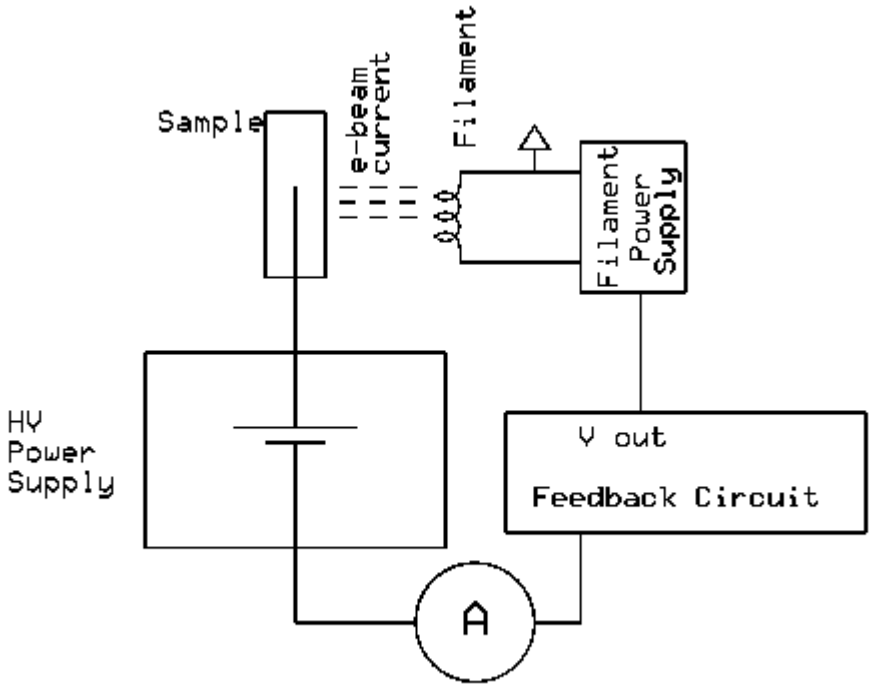

Fig 4.1 – The e-beam heater circuit. The current between the sample and the filament must be held constant. The feedback circuit reads the current and outputs a voltage to a programmable input on the filament power supply. This input reads the voltage and alters the voltage across the filament maintaining the current at a constant value.

In order to maintain a constant rate of evaporation a constant current must be maintained between the filament and the source. This is accomplished by means of installing a feedback loop between the circuit and the power supply for the filament. This feedback loop analyzes the current and changes the voltage across the filament to maintain the constant current. Without the feedback loop the current would continually fluctuate due to the changing resistance of the filament as it is heated. This in turn would produce an uneven deposition rate which can cause problems in the structure of the thin films. My goal in this project was to build and test the feedback circuit to be used in the e-beam heater.

4.1 The Feedback Circuit

The circuit was designed by Mike Grobis and Annie Endozo at the University of California at Berkeley. More information on the circuit can be found in Appendix D. A program called ExpressPCB[6] was used to design the actual circuit board that was to be printed. This program was equipped with a series of footprints for standard electronic components and allowed for easy manipulation of these components on the board. All the components were arranged in a logical fashion on the board that minimized the area. Once all the footprints were placed on the board the diagram was linked to the circuit diagram created in a sister program by the name of ExpressSCH. This link facilitated the process of connecting all the pieces by highlighting connections that needed to be made. Traces were drawn between all the vias that were on the board connecting the components and completing the circuit. A common point for the power source was also supplied to the board to power the opamps. Inputs and outputs were added to later be connected to BNC inputs mounted on the box.

The circuit was designed as a two layer board. The top layer, colored red in the diagram below, contains all the traces that connect the various components. It is to this layer also that the input and the output are attached. The bottom layer has been constructed as a grounding layer, colored green in the diagram below. The entire bottom of the board is grounded except for those places where holes for components lay. These spaces are surrounded with a small open area to keep the points from being grounded. Components that were to be grounded had traces run from their holes to the surrounding

ground layer. The outline of the board can be seen in the yellow lines of the diagram. The board only measures 3.8” x 2.5”. The board itself is made of a thick insulating material.

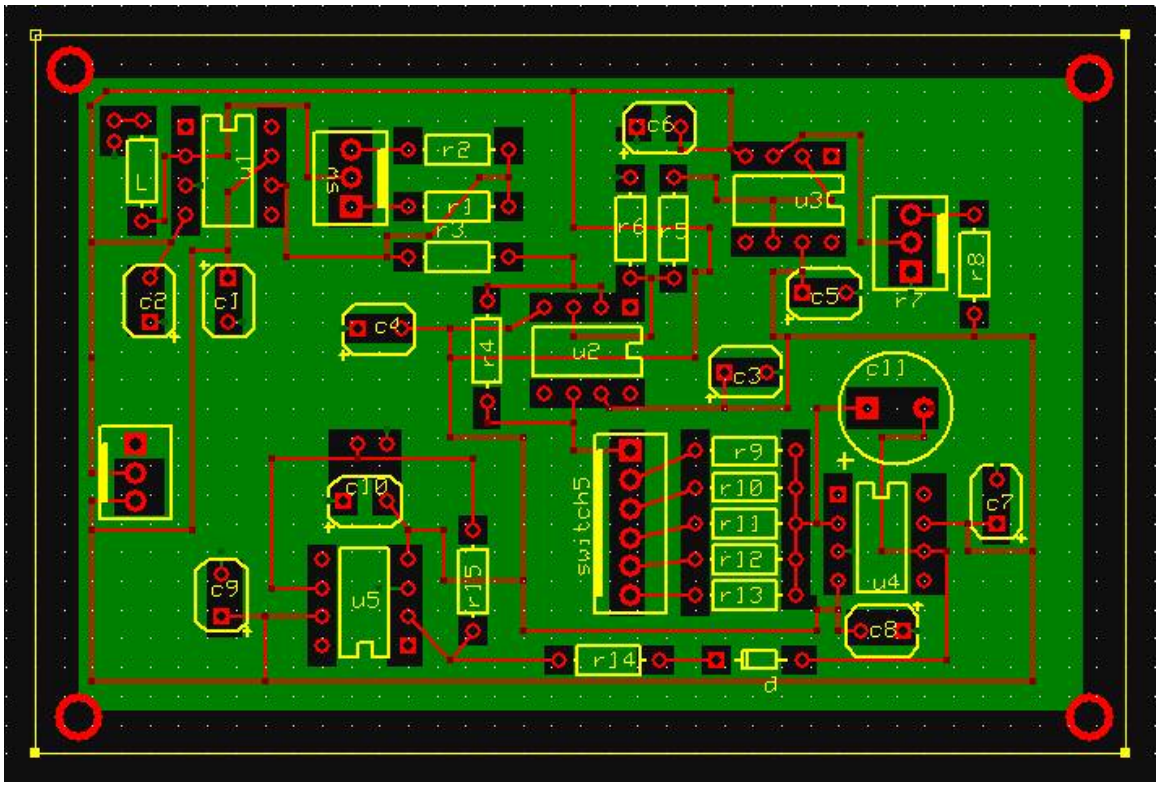

Figure 4.2 – Layout of the board for the feedback circuit. The green represents the bottom grounding copper layer, while the red represents the top copper layer. The yellow layer is for reference but is not an actual part of the board.

Standard components were installed on the board. The resistors are all ¼ watt axial resistors. The capacitors running off all of the opamps are tantalum radial capacitors with a capacitance of 0.10 µF. These capacitors all have a polarization direction marked on the component. The opamps are OP27s operating with a voltage of ± 15 V. The diode is an IN4448 forward biased diode. The lone capacitor not running off an opamp, C11 in the diagram, is a radial capacitor with a capacitance of 2.2 µF. Standard three and six pin connectors were used for the switches, turnpot and the power supply.

Once the board layout was finalized the board was assembled, soldering all the components in the appropriate locations. The power for the circuit is provided by a small power source located on the inside of the box. It outputs ± 15 V DC with a current of 0.10 A. There are three different switches used on the box (figure 4.3).

Figure 4.3 – The front panel of the feedback box.

The first, located in the upper left hand corner of the face of the box, controls the power for the box. It has an LED inserted in the switch indicating when the circuit is on or off. The second switch controls the gain for the first opamp. This switch is located in the bottom left hand corner of the box and an up and a down position. The final switch in the system is a 5 pin switch that allows us to choose the time constant for the integrator. The knob has five positions and a small arrow to mark which position is being used. Also on the face of the box are two BNC female connectors. These are connected to the input and output of the circuit. A large ten turn dial is located on the upper right hand corner of the

box. This controls the turnpot and allows us to accurately mark the setpoint for the circuit. Each full revolution of the dial turns a small counter on the top of the dial allowing us to keep track of the number of turns. A small lock is located on the bottom of the dial allowing us to lock the setpoint in. The only connector on the back of the box is the standard 110/120 V AC outlet. This will provide power to the power supply located in the box.

Figure 4.4 – The finished box housing the feedback circuit.

The finished product can be seen in figure 4.4. This box will then be connected to negative terminal of the high voltage power supply and the power supply for the filament loop. This establishes the feedback loop in the e-beam heater.

4.2 Testing of the Circuit

Once the circuit was completely built it was tested. The test was performed was using an input of a slowly oscillating (<1 Hz) sine wave. The input was split and connected to the box and to one probe of an oscilloscope. The output from the box was connected to the second probe of the oscilloscope. When the box was first attached the output did not seem to behave in the correct manner. Using a digital multimeter (DMM) we followed the input around the circuit. Everything behaved as expected in the circuit up until the point of the integrator (see Figure D.1, opamp #4).

When the output of this opamp was examined, the result was always about 14 volts. The integrator was being saturated because it had no finite dc feedback for stable biasing. This problem was solved by adding a 10 MΩ resistor in parallel to the capacitor across the integrator opamp (C11 in figure D.1).

Once this was done the circuit began to behave very nicely. The input of a slow (~5 HZ) sine wave produced an inverted sine wave of the same frequency.

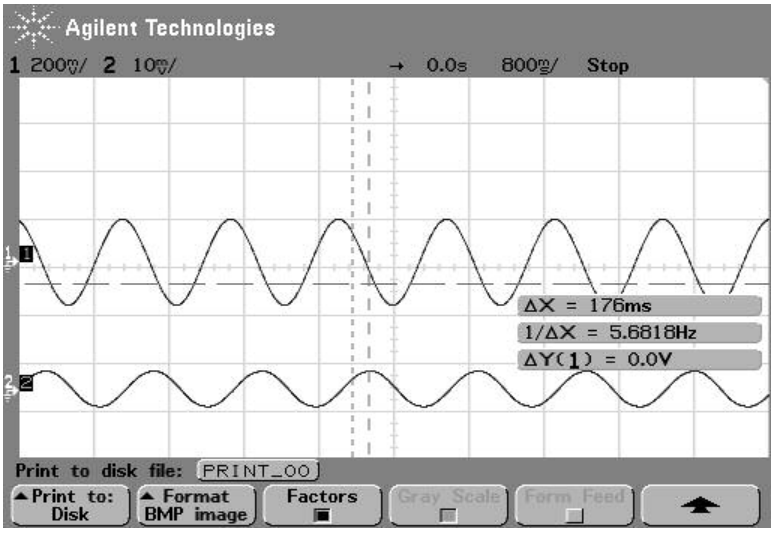

Figure 4.5 – The oscilloscope display of the feedback circuit. The bottom display is the input sine wave and the top display is the resulting output.

From the figure above we can see that the feedback circuit is responding to the changing input signal. As the input decreases the output increases, and vice versa. The circuit is working to attain a steady signal. This will control and maintain a constant current in the

e-beam heater allowing us to have uniform deposition.

Appendix A

Theory of Scanning Tunneling Microscopy[7]

An STM operates by bringing a very sharp metal tip to within a few angstroms of the surface of the sample. At this point the tip is close enough to the sample to allow for tunneling to occur between the tip and the surface. If no voltage is applied between the tip and the surface, electrons in the surface and the tip will flow back and forth until an alignment of their Fermi levels has been achieved. This is the steady state.

In order to ensure that there is a constant flow of electrons between the tip and the surface a small bias voltage is applied between the two. This serves to raise the Fermi level of the tip to just slightly above that of the surface thus creating an imbalance that causes the electrons to flow. The bias voltage can also be applied to the sample causing electrons to flow in the opposite direction. These tunneling electrons produce a current that is measurable. Imaging can be reproduced by two methods. The tip of the STM can be held at a constant height and the corresponding changes in voltage can be mapped to create a topographic map of the sample. Alternatively the tunneling current can be held constant and the changes in the height of the tip can be mapped to create the image. This method tends to be preferred because it protects the tip from running into the surface of the sample.

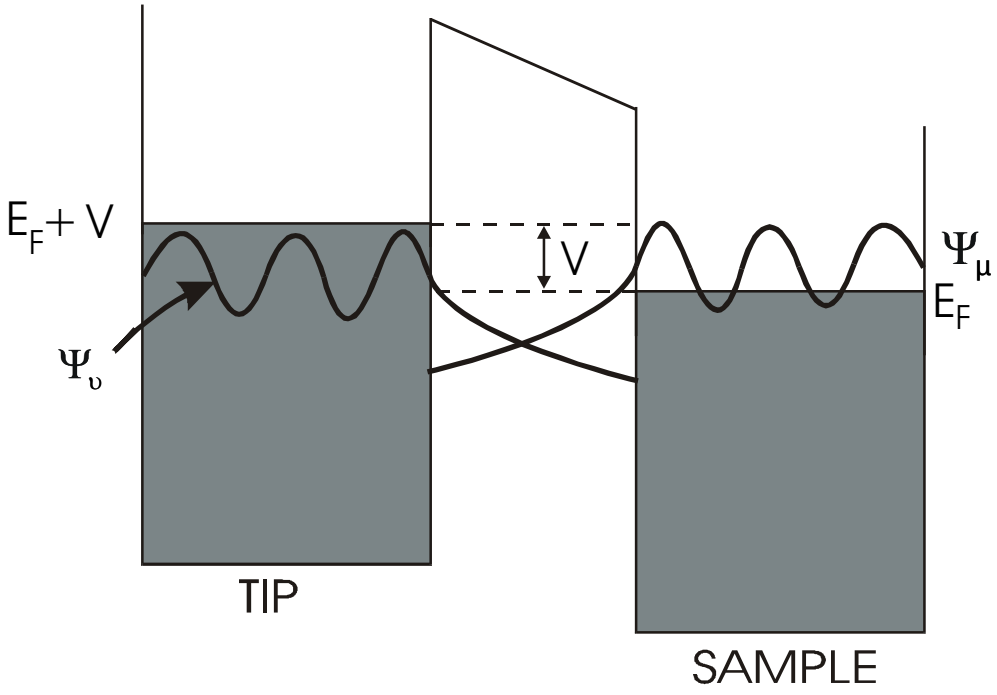

Fig A.1 Tunneling from the tip to the sample across a vacuum.[8]

The theory that accompanies this model was first created by Bardeen[9] in 1960 and later modified and adapted for STM by Tersoff and Hamann[10]. Both the tip and the sample are treated as having separate local density of states (DOS) that are in contact with each other. If we assume that the energy is conserved throughout the tunneling process then the current will depend on the DOS of the tip and the sample as

$$I = I_{sample \to tip} - I_{tip \to sample} \tag{A.1}$$

$$= \frac{4\pi e}{\hbar} \int_{-\infty}^{\infty} |M|^2 \rho_s(E_s)\rho_t(E_t)\{f(E_s)[1-f(E_t)] - f(E_t)[1-f(E_s)]\} d\varepsilon \tag{A.2}$$

In this equation M is the tunneling matrix element, ρ is the density of states and f is the Fermi function given by $f(E) = \{1+\exp[(E - E_F)/K_B T]\}^{-1}$. In simple terms this equation says that there must be a state to tunnel from and a state to tunnel to in order for there to be a current.

In order for the energy to be conserved then E_s and E_t must be equal. It is then possible to rewrite the current in terms of the energy level with respect to the Fermi level

E_F. In this case, since the two are separated by the bias voltage applied to the tip, the energies are written as $E_s = \varepsilon$ and $E_t = \varepsilon + eV$ and we are left with

$$I = \frac{4\pi e}{\hbar}\int_{-\infty}^{\infty}|M|^2 \rho_s(\varepsilon)\rho_t(\varepsilon + eV)[f(\varepsilon) - f(\varepsilon + eV)]d\varepsilon \quad \text{(A.3)}$$

It was shown by Bardeen though in his framework that the tunneling matrix element could be expressed as

$$M_{\mu\upsilon} = \frac{\hbar^2}{2m}\int_{\rho} dS.(\Psi_\mu^*\nabla\Psi_\upsilon - \Psi_\upsilon\nabla\Psi_\mu^*) \quad \text{(A.4)}$$

The integral in this equation is done over any surface that is entirely in the vacuum barrier. It is possible to calculate the value of this integral if the assumption is made that the dominant interaction comes from the s-wave functions of the tip. This will give us

$$I \sim \sum_{\mu}|\Psi_\mu(r_0)|^2 \delta(E_\mu - E_\upsilon - ev) \quad \text{(A.5)}$$

which can then be reduced to

$$I \sim e^{-2\kappa d} \quad \text{(A.6)}$$

Thus it is seen that the tunneling current is exponentially dependent upon the separation d of the tip from the sample, and κ, which is the exponential decay length and is defined as

$$\kappa = \sqrt{\frac{2m\varphi}{\hbar^2}} \quad \text{(A.7)}$$

Here φ represents the work function. For most metals the work function has been determined to be in the range of a few eV, from which a simple calculation shows us that the current is exponentially sensitive to length scales on the order of angstroms. If we were to assume a work function of 4 eV and we increase the distance between the sample an the tip by 1 angstrom, we see

$$2\kappa d = 2 * \sqrt{\frac{2 * 9.11 * 10^{-31} * 4 * 1.602 * 10^{-19}}{(1.054 * 10^{-34})^2}} * 10^{-10} \approx 2 \quad \text{(A.8)}$$

This result indicates that the current will drop by a factor of e^{-2}, which is roughly 0.135. So the difference of a single angstrom is dropping the current by almost a factor of 10. It is this dependence that allows for the extraordinary resolution offered by the STM.

Appendix B

Theory and History of Piezoelectricity[11]

B.1 History

Piezoelectricity was first discovered around 1880 by the Curie brothers. The experiment used to confirm its existence consisted of the measurement of charge generated along the surface of specially prepared crystals when a mechanical stress was applied to the crystal. The effect was deduced by the brothers as a result of the symmetry, or more importantly the asymmetry, of the crystal. It was this thinking that had led them to prepare certain crystals, cut in a specified manner, such as quartz and Rochelle salt. By definition the term piezoelectric effect refers only to the production of a voltage as induced my mechanical stress. It was only discovered a year later, by a mathematician Lippmann, that the converse effect must also be present. That is to say that when these crystals are placed in an electric field oriented in the proper direction, they induce a mechanical stress. This effect is sometimes referred to as the converse piezoelectric effect. Shortly after its deduction the Curie brothers successfully proved its existence in the laboratory.

There was some work in the field in the following years but because the mechanical stress and charges involved were so small in magnitude few applications were discovered that could take advantage of these properties. It would not be until the middle of World War I that the piezos application in techniques such as sonar detection of submarines would become apparent. Today piezoelectric materials are used in a whole host of applications. They can be found in a variety of technical equipment and in products as simple as lighters. They have completely permeated society.

B.2 The Piezoelectric Effect

The piezoelectric effect is purely the result of the asymmetry of the crystal and is not a product of the crystal itself. There are a possible 32 crystal classes by which a crystal can be constructed. Of these possible 32 classes, 15 are centrosymmetric, that is

they can be inverted and are structurally equivalent, and thus exhibit none of the piezoelectric properties. One other configuration is also ruled out by means of a more complicated symmetry argument. Thus there are a total of 20 different crystal structures that are able to exhibit piezoelectric properties.

The mathematical definition of the piezoelectric relationships are

$$P_i = \sum_{j,k} d_{ijk} \sigma_{jk} \tag{B.1}$$

$$e_{jk} = \sum_{i} d_{ijk} E_i \tag{B.2}$$

Where P is the polarization, σ is the applied stress, e is the strain, E is the electric field and d is the piezoelectric constant. The units of d are C/N or equivalently m/V depending on the situation. d has a possible 27 components but due to symmetry relations only 18 of them are independent and have to be considered. Many of the components are often zero thus simplifying calculations further.

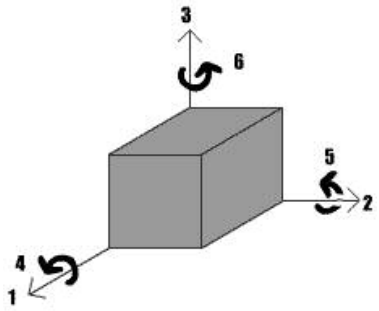

Figure B.1 – Each of the orthogonal axes are referenced by the numbers 1, 2 and 3. The numbers 4,5 and 6 refer to shear motion about the corresponding axis.

Sometimes the relationship is represented in matrix notation. The axis notation used is represented in the figure above and allows us to take advantage of certain symmetries.

$$\begin{bmatrix} P_1 \\ P_2 \\ P_3 \end{bmatrix} = \begin{bmatrix} d_{11} & d_{12} & d_{13} & d_{14} & d_{15} & d_{16} \\ d_{21} & d_{22} & d_{23} & d_{24} & d_{25} & d_{26} \\ d_{31} & d_{32} & d_{33} & d_{34} & d_{35} & d_{36} \end{bmatrix} \begin{bmatrix} \sigma_1 \\ \sigma_2 \\ \sigma_3 \\ \sigma_4 \\ \sigma_5 \\ \sigma_6 \end{bmatrix} \tag{B.3}$$

$$\begin{bmatrix} e_1 \\ e_2 \\ e_3 \\ e_4 \\ e_5 \\ e_6 \end{bmatrix} = \begin{bmatrix} d_{11} & d_{21} & d_{31} \\ d_{12} & d_{22} & d_{32} \\ d_{13} & d_{23} & d_{33} \\ d_{14} & d_{24} & d_{34} \\ d_{15} & d_{25} & d_{35} \\ d_{16} & d_{26} & d_{36} \end{bmatrix} \begin{bmatrix} E_1 \\ E_2 \\ E_3 \end{bmatrix} \tag{B.4}$$

In the case of the shear piezo used in the experiment the resultant matrix takes the following form.

$$\begin{bmatrix} e_1 \\ e_2 \\ e_3 \\ e_4 \\ e_5 \\ e_6 \end{bmatrix} = \begin{bmatrix} 0 & 0 & d_{31} \\ 0 & 0 & 0 \\ 0 & 0 & d_{33} \\ 0 & 0 & 0 \\ d_{15} & 0 & 0 \\ 0 & 0 & 0 \end{bmatrix} \begin{bmatrix} E_1 \\ 0 \\ 0 \end{bmatrix} \tag{B.5}$$

The equation is greatly simplified in this instance allowing for calculations to be performed quite easily. Only one component of the strain is non zero, $e_{5,}$ giving us the following simple relation for our shear piezos.

$$e_5 = d_{15} E_1 \tag{B.6}$$

This means that an electric field applied along the 1 direction will produce a shear about the 2 direction.

The actual effect of piezoelectricity is the result of the displacement of the atoms inside of the crystal. A piezoelectric crystal free from stress or an applied field has an internal balance of charges. These charges are perfectly balanced by the symmetry of the crystal. As an electric field is applied or a mechanical stress is induced, the symmetry of the crystal is broken and the charges are no longer aligned. In the case of the mechanical stress being applied, the charges now exhibit an electric field. In the case of the applied

electrical field the charges are affected by the field altering the structure of the crystal. This structure alteration results in a deformation of the crystal

The direction of these movements and fields is purely a result of the structure of the original crystal. Single motions or combinations of motions can be achieved in a single crystal depending upon the structure. Piezos that grow, shrink, shear and any combination of the above can be created.

In the case of the shear piezos used in the STM, there are a total of eight possible orientations in which to use the piezos. These possible orientations along with the resultant motion have been outlined in the diagram below.

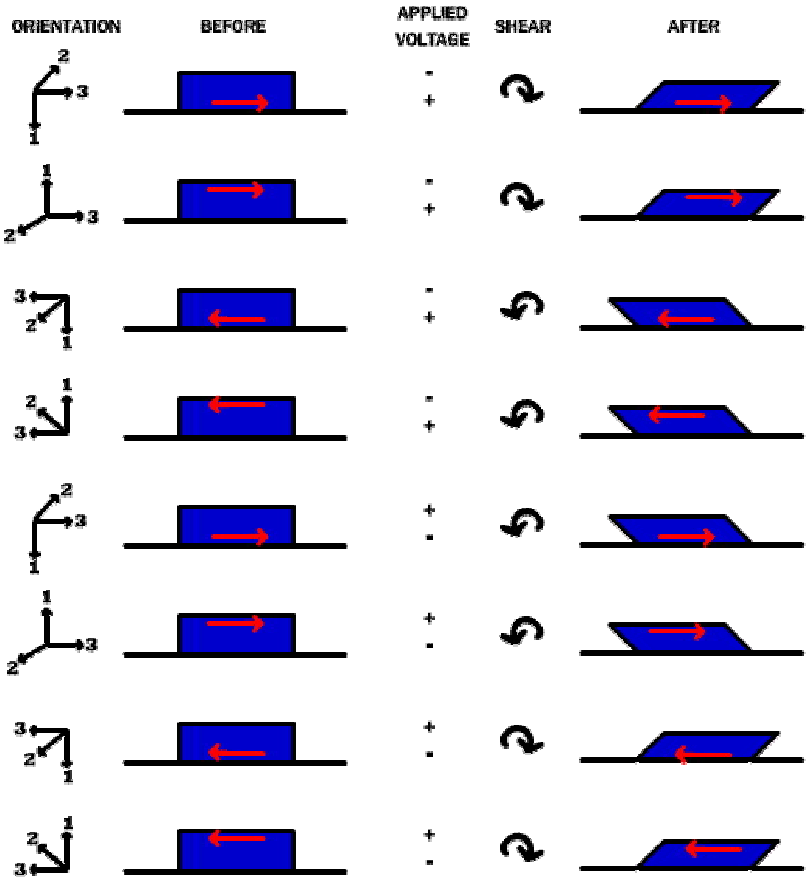

Figure B.2 – The 8 possible orientations of the shear piezoelectric pieces used in this experiment

B.3 Piezoelectric Materials

Because piezoelectricity is purely a function of the crystal structure it has no connection to the material involved. Some materials exhibit the effect with simply the correct preparation, such as cutting along a certain plane. Quartz and Rochelle Salt were two of the earliest materials discovered with this effect. Recently many more materials have been fabricated that also exhibit this effect. The most common are lead zirconium titanates, or PZTs. This ceramic has a crystal structure filled with dipoles. It is because of this that the PZT needs to be poled to ensure that the direction of motion is uniform. If the material is not poled then the motion can be unpredictable and erratic.

Poling is achieved normally through heating the sample and applying a very strong magnetic field. This field aligns all the dipoles in a certain direction which when the field is removed the ceramic retains. This provides a direction of polarization in the material. One must be careful not to apply too strong of an electric field to these piezos or they can be depoled. If an electric field of sufficient strength is applied to the piezo it randomizes the alignments of the dipoles. This depoling voltage is a function of the geometry of the crystal and the material.

Appendix C

Piezoelectric Test Results

Piezo	Configuration	Fringe movement	# of fringes for -350 V
2	← Towards laser	Inward	~ ½ fringe
	→ Away from laser	Outward	¾ to 1 fringe
	↑ Towards screen	Outward	Just noticeable
4	← Towards laser	Inward	~ 1 fringe
	→ Away from laser	Outward	~ 1 fringe
	↑ Towards screen	—	None
8	← Towards laser	Inward	~ ⅓ fringe
	→ Away from laser	Outward	~ ¾ fringe
	↑ Towards screen	Inward	Just noticeable
10	← Towards laser	Inward	~ ½ fringe
	→ Away from laser	Outward	~ 1 ¼ fringe
	↑ Towards screen	—	None
11	← Towards laser	Inward	~ 1 ¼ fringe
	→ Away from laser	Outward	< ½ fringe
	↑ Towards screen	Outward	~1 ¼ fringe
12	← Towards laser	Outward	~ ½ fringe
	→ Away from laser	Outward	Barely noticeable
	↑ Towards screen	Inwards	Barely noticeable
13	← Towards laser	Inward	¾ fringe
	→ Away from laser	Outward	¾ fringe
	↑ Towards screen	—	None
15	← Towards laser	Inward	~ 1 fringe
	→ Away from laser	Outward	~ 1 fringe
	↑ Towards screen	—	None
17	← Towards laser	Inward	~ ½ fringe
	→ Away from laser	Outward	~ ½ fringe
	↑ Towards screen	Inward	Justnoticeable
20	← Towards laser	Inward	~ 1 fringe
	→ Away from laser	Outward	~ 1 fringe
	↑ Towards screen	Outward	Just noticeable
23	← Towards laser	Inward	~ 1 fringe
	→ Away from laser	Outward	~ 1 fringe
	↑ Towards screen	—	None
26	← Towards laser	Inward	~ 1 fringe
	→ Away from laser	Outward	1 ¼ fringe
	↑ Towards screen	Outward	< ¼ fringe
27	← Towards laser	Inward	~ ¾ fringe
	→ Away from laser	Outward	~ ¾ fringe
	↑ Towards screen	Outward	Just noticeable

29	← Towards laser	Inward	~ ½ fringe
	→ Away from laser	Outward	~ ¾ fringe
	↑ Towards screen	—	None
31	← Towards laser	Inward	~ 1 fringe
	→ Away from laser	Outward	~ ¾ fringe
	↑ Towards screen	Outward	< ¼ fringe
32	← Towards laser	Inward	~ ¾ fringe
	→ Away from laser	Outward	~ ¾ fringe
	↑ Towards screen	Outward	< ¼ fringe
33	← Towards laser	Inward	~ 1 fringe
	→ Away from laser	Inward	< ¼ fringe
	↑ Towards screen	Outward	~ 1 fringe
34	← Towards laser	Inward	¾ to 1 fringe
	→ Away from laser	Outward	~ ¼ fringe
	↑ Towards screen	Outward	¾ to 1 fringe
36	← Towards laser	Inward	½ to ¾ fringe
	→ Away from laser	Outward	¾ to 1 fringe
	↑ Towards screen	—	None
37	← Towards laser	Inward	~ 1 fringe
	→ Away from laser	Outward	< ¼ fringe
	↑ Towards screen	Outward	> 1 fringe
38	← Towards laser	Inward	~ ½ fringe
	→ Away from laser	Outward	~ ¾ fringe
	↑ Towards screen	Outward	Barely noticeable
39	← Towards laser	Inward	~ ¾ fringe
	→ Away from laser	Outward	~ ¾ fringe
	↑ Towards screen	—	None
40	← Towards laser	Inward	¾ to 1 fringe
	→ Away from laser	Outward	¾ fringe
	↑ Towards screen	—	None
46	← Towards laser	Inward	~ ½ fringe
	→ Away from laser	Outward	~ ¾ fringe
	↑ Towards screen	—	None
47	← Towards laser	Inward	¾ to 1 fringe
	→ Away from laser	Outward	¼ to ½ fringe
	↑ Towards screen	Inward	~ 1 fringe
49	← Towards laser	Inward	~ ¾ fringe
	→ Away from laser	Outward	~ ¾ fringe
	↑ Towards screen	Inward	~ ½ fringe
50	← Towards laser	Inward	~ ¾ fringe
	→ Away from laser	Outward	~ ¾ fringe
	↑ Towards screen	Inward	< ¼ fringe
N1	← Towards laser	Inward	~ 1 fringe
	→ Away from laser	Inward	~ ½ fringe
	↑ Towards screen	Outward	~ 1 fringe

N8	← Towards laser	Inward	½ to ¾ fringe
	→ Away from laser	Outward	¾ fringe
	↑ Towards screen	—	None
N10	← Towards laser	Inward	~ ¼ fringe
	→ Away from laser	Outward	¼ to ½ fringe
	↑ Towards screen	Inward	¼ fringe
N11	← Towards laser	Inward	~ ½ fringe
	→ Away from laser	Outward	~ ½ fringe
	↑ Towards screen	—	None
N13	← Towards laser	Inward	~ ½ fringe
	→ Away from laser	Outward	¾ to 1 fringe
	↑ Towards screen	—	None
N15	← Towards laser	Inward	½ to 34 fringe
	→ Away from laser	Outward	~ 1 fringe
	↑ Towards screen	—	None
N17	← Towards laser	Inward	¼ to ½ fringe
	→ Away from laser	Outward	½ to ¾ fringe
	↑ Towards screen	—	None
N19	← Towards laser	Inward	¾ to 1 fringe
	→ Away from laser	Outward	~ ¾ fringe
	↑ Towards screen	Outward	< ¼ fringe
N21	← Towards laser	—	None
	→ Away from laser	Outward	½ to ¾ fringe
	↑ Towards screen	Inward	~ ¾ fringe
N22	← Towards laser	Outward	1 ¼ fringe
	→ Away from laser	Inward	1 ¼ fringe
	↑ Towards screen	Outward	1 ½ fringe
N23	← Towards laser	Inward	~ 1 fringe
	→ Away from laser	Outward	1 to 1 ¼ fringe
	↑ Towards screen	—	None
N24	← Towards laser	Inward	~ ¾ fringe
	→ Away from laser	Outward	½ to ¾ fringe
	↑ Towards screen	Outward	Just noticeable

Appendix D

Explanation of the Feedback Circuit

The feedback circuit that we used in this system was designed by Mike Grobis and Annie Endozo at the University of California at Berkeley. It can be seen in the diagram below.

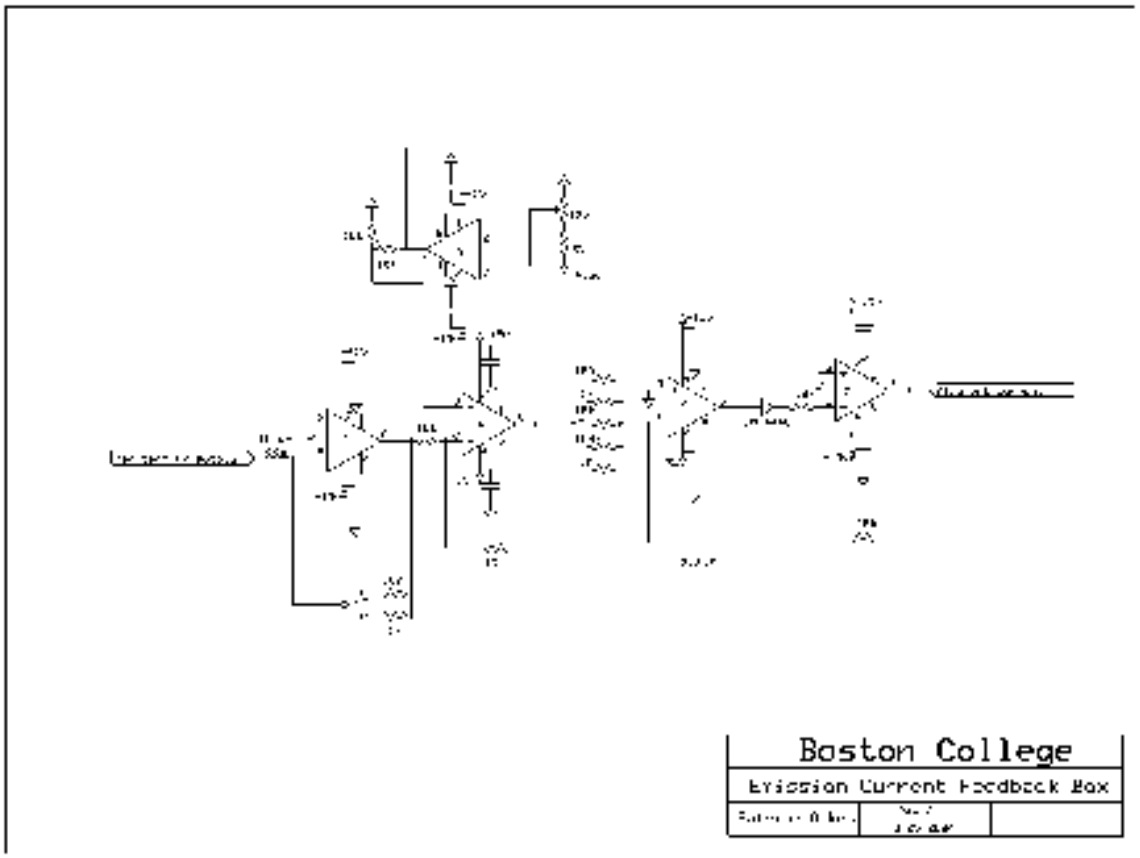

Figure D.1 – Feedback circuit schematic.

The input is from the negative terminal of the high voltage power supply. The first opamp in the circuit converts the signal from a current to a voltage. There is a switch attached to this opamp allowing us to choose the gain. The 10K turnpot in the center of the top of the diagram allows us to create a setpoint for which to compare the input signal

to. The 5K resistor is attached to the turnpot to ensure that if the turnpot is set to 0, the circuit does not experience a large voltage drop causing damage to the circuit. The second opamp in the circuit takes the voltage determined by the turnpot and inverts it so it can be compared to the input signal.

The third opamp is set up as a differentiator. This will take the two signals, the input and the setpoint, and compare them taking the difference between the two signals. There is no gain at this opamp. The signal at this point is sent through a switch that allows us to determine the time constant for the integrator which is the function of opamp four. The signal is then passed through a forward biased diode to ensure that the signal has the correct positive sign. The final opamp then takes the signal and inverts it again to a negative voltage.

This output is then sent to a programmable input on the power supply for the filament. That input interprets the signal and accordingly adjusts the voltage being passed through the filament to ensure that the current between the filament and the source is maintained at a constant value.

References

[1] G. Binnig, H. Rohrer, Ch. Gerber and E. Weibel. *Surface Studies by Scanning Tunneling Microscopy*. Phys. Rev. Lett. **49,** 57. (1982)

[2] V. Madhavan. Transition Metal Atoms and Clusters on a AU(111) Surface: An STM Study. Boston University. 2000. p 10.

[3] Figure is combined from two sources:
V. Madhavan. Transition Metal Atoms and Clusters on a AU(111) Surface: An STM Study. Boston University. 2000. p 15.
E. Hudson. *Investigating High-T_C Superconductivity on the Atomic Scale by Scanning Tunneling Microscopy*. University of California at Berkeley. 1999. p 2.

[4] Performed by Chang-Jin Lee

[5] Nor-Cal 2004 catalogue

[6] Program is the copyright of ExpressPCB. Information can be found at www.expressPCB.com

[7] Summary from
V. Madhavan. Transition Metal Atoms and Clusters on a AU(111) Surface: An STM Study. Boston University. 2000.
E. Hudson. *Investigating High-T_C Superconductivity on the Atomic Scale by Scanning Tunneling Microscopy*. University of California at Berkeley. 1999.

[8] V. Madhavan. Transition Metal Atoms and Clusters on a AU(111) Surface: An STM Study. Boston University. 2000. p 32.

[9] J. Bardeen. *Tunneling from a Many-body Point of View*. Phys. Rev. Lett. **6**, 57-59. (1960)

[10] J. Tersoff and D.R. Hamann. *Theory and Application for the Scanning Tunneling Microscope*. Phys. Rev. Lett. **50**, 25. (1983)

[11] Summary from W. Cady. *Piezoelectricty*. McGraw-Hill, New York. 1946.